



Article

Porphyromonas gingivalis Strain W83 Infection Induces Liver Injury in Experimental Alcohol-Associated Liver Disease (ALD) in Mice

Yun Zhou ^{1,2,*}, Craig McClain ^{1,2,3,4,5}  and Wenke Feng ^{1,2,3,5,6,*}¹ Department of Medicine, University of Louisville, Louisville, KY 40202, USA; craig.mcclain@louisville.edu² Alcohol Research Center, University of Louisville, Louisville, KY 40202, USA³ Hepatobiology and Toxicology Center, University of Louisville, Louisville, KY 40202, USA⁴ Robley Rex VA Medical Center, Louisville, KY 40202, USA⁵ Department of Pharmacology and Toxicology, University of Louisville, Louisville, KY 40202, USA⁶ Department of Structural and Cellular Biology, Tulane University, New Orleans, LA 70112, USA

* Correspondence: zhou.zyun@gmail.com (Y.Z.); wfeng@tulane.edu (W.F.); Tel.: +1-5049885232 (W.F.)

Abstract: The liver plays a vital role in the defense against infections. *Porphyromonas gingivalis* (*P. gingivalis*), a dominant etiologic oral bacterium implicated in periodontal disease (PD), has been associated with various systemic diseases. This study aimed to investigate the influence of *P. gingivalis* on alcohol-associated liver diseases (ALD). Mice were fed a Lieber–DeCarli liquid diet containing 5% ethanol for 10 days after an initial adaptation period on a diet with lower ethanol content for 7 days. Two days before tissue sample collection, the mice were administered *P. gingivalis* strain W83 (*Pg*) through intraperitoneal injection (IP). Pair-fed mice with *Pg* infection (PF+*Pg*) exhibited an activated immune response to combat infections. However, alcohol-fed mice with *Pg* infection (AF+*Pg*) showed liver injury with noticeable abscess lesions and elevated serum alanine aminotransferase (ALT) levels. Additionally, these mice displayed liver infiltration of inflammatory monocytes and significant downregulation of proinflammatory cytokine gene expression levels; and AF+*Pg* mice also demonstrated increased intrahepatic neutrophil infiltration, as confirmed by chloroacetate esterase (CAE) staining, along with elevated gene expression levels of neutrophil cytosol factor 1 (*Ncf1*), neutrophilic inflammation driver lipocalin 2 (*Lcn2*), and complement component C5a receptor 1 (*C5ar1*), which are associated with neutrophilic inflammation. Interestingly, compared to PF+*Pg* mice, the livers of AF+*Pg* mice exhibited downregulation of gene expression levels of NADPH oxidase 2 (*Cybb*), the leukocyte adhesion molecule *Cd18*, and the Toll-like receptor adaptor *Myd88*. Consequently, impaired clearance of *P. gingivalis* and other bacteria in the liver, increased susceptibility to infections, and inflammation-associated hepatic necrotic cell death were observed in AF+*Pg* mice, which is likely to have facilitated immune cell infiltration and contributed to liver injury. Furthermore, in addition to the *Srebf1/Fasn* pathway induced by alcohol feeding, *Pg* infection also activated carbohydrate response element-binding protein (*ChREBP*) in AF+*Pg* mice. In summary, this study demonstrates that *P. gingivalis* infection, acting as a “second hit”, induces dysfunction of immune response and impairs the clearance of bacteria and infections in alcohol-sensitized livers. This process drives the development of liver injury.

Keywords: alcohol-associated liver disease; *P. gingivalis*; inflammatory monocyte infiltration; intrahepatic neutrophil infiltration; hepatic steatosis; liver injury



Citation: Zhou, Y.; McClain, C.; Feng, W. *Porphyromonas gingivalis* Strain W83 Infection Induces Liver Injury in Experimental Alcohol-Associated Liver Disease (ALD) in Mice. *Appl. Microbiol.* **2024**, *4*, 620–634. <https://doi.org/10.3390/applmicrobiol4020043>

Academic Editors: Serena Schippa and Sanna Maria Sillankorva

Received: 19 February 2024

Revised: 19 March 2024

Accepted: 24 March 2024

Published: 27 March 2024



Copyright: © 2024 by the authors. Licensee MDPI, Basel, Switzerland. This article is an open access article distributed under the terms and conditions of the Creative Commons Attribution (CC BY) license (<https://creativecommons.org/licenses/by/4.0/>).

1. Introduction

Alcohol-associated liver disease (ALD) is a significant global health concern, contributing to substantial morbidity, mortality, and healthcare costs. ALD encompasses a spectrum of liver conditions resulting from excessive alcohol consumption, ranging from simple fatty liver (steatosis) to more severe forms, such as alcohol-associated steatohepatitis (AH),

cirrhosis, and even hepatocellular carcinoma [1,2]. In 2012, about 3.3 million deaths, or 5.9% of all global deaths, were attributed to alcohol consumption [2]. In 2017, an estimated 23.6 million people globally had alcohol-associated cirrhosis, with approximately 10% of these having decompensated disease [3]. In the United States, up to 1% of the population may have ALD [4]. ALD is often complicated by concomitant diseases, including viral infections. Emerging evidence suggests an association between ALD and periodontal disease (PD) [5]. In patients with ALD, viral and bacterial infections are frequently observed, acting as potential “second hits” or multiple hits that contribute to the progression of ALD [6].

One of the major pathogens associated with PD is *Porphyromonas gingivalis* (*P. gingivalis*). *P. gingivalis* has virulence factors, such as gingipains, capsular polysaccharide, fimbriae and outer membrane vesicles, which invade host immune responses [7,8]. This bacterium can evade elimination by the complement system [9,10] and can translocate from dental plaque to other organs, either through circulation or oral infection that exacerbates various diseases, such as arthritis, cardiovascular disease, diabetes, and Alzheimer’s disease [11–13]. *P. gingivalis* has been considered a confounding risk factor for systemic diseases when not efficiently eliminated by the host. Our previous study demonstrated an association between *P. gingivalis* and the development/severity of acute alcohol-associated steatohepatitis (AAH) [14]. However, whether *P. gingivalis* infection directly causes liver damage after alcohol consumption remains to be demonstrated.

In this current study, we aimed to investigate whether *P. gingivalis* infection, as a “second hit”, could promote the development and progression of ALD. We also sought to explore the underlying molecular mechanisms involved. Using a virulent strain of *P. gingivalis* known as W83 (*Pg*), which is a key contributor to PD [15,16], we conducted experiments in mice. We hypothesized that systemic *Pg* infection, likely to stem from the dysbiosis of the oral microbiome, caused liver injury by inducing infiltration of immune cells into the liver and exacerbated alcohol-induced liver inflammation in patients with ALD.

2. Materials and Methods

2.1. Animals Fed with Alcohol

C57BL/6J male mice (age 8 weeks, weight 25–30 g) were purchased from Jackson Laboratory (Bar Harbor, ME). They were maintained at 22 °C with a 12 h light/dark cycle and had free access to a normal chow diet and tap water for one week. Afterwards, mice were divided into 2 groups and fed with either a Lieber–DeCarli liquid diet or a maltose–dextrin pair-fed diet. For alcohol-feeding (AF), mice were fed for one day with control diet (BioServ, Flemington, NJ, USA), 3 days with 1.6% ethanol diet (1.6% ethanol in ethanol diet BioServ), 3 days with 3.2% ethanol diet, and 10 days with 5% ethanol diet. For pair-feeding (PF), mice were fed with isocaloric control diet (Figure 1) [17,18]. All mice were treated according to the protocols reviewed and approved by the Institutional Animal Care and Use Committee of the University of Louisville (approval number: 18378), and all the procedures were carried out in accordance with the approved guidelines.

2.2. Bacteria Preparation and Mouse Treatment

The *P. gingivalis* strain W83 (*Pg*) was purchased from the ATCC (Manassas, VA) and re-suspended in sterile PBS at a concentration of 2×10^9 CFU (colony-forming units)/mL. Two days before the end of experiment, mice were infected with the bacteria by intraperitoneal injection (IP) of 100 μ L *Pg* (total 2×10^8 CFU/ animal). Mice in control groups (non-infection groups) were injected with 100 μ L PBS. Thirty mice were divided into 4 groups with each group containing 7–8: pair-fed (PF), pair-fed with *P. gingivalis* infection (PF+*Pg*), alcohol-fed (AF) and alcohol-fed with *P. gingivalis* infection (AF+*Pg*). Due to mortality loss during alcohol and *Pg* challenge, the final numbers of mice in each group were: PF (7); PF+*Pg* (7), AF (6), and AF+*Pg* (6). The body weights of mice were measured daily. Forty-eight hours after *Pg* infection, mice were anesthetized with avertin and sacrificed. Mouse blood samples were collected and allowed to clot at room temperature for 30 min

and were centrifuged at $1500\times g$ for 30 min to collect serum. Mouse liver and spleen samples were weighted and collected for various assays.

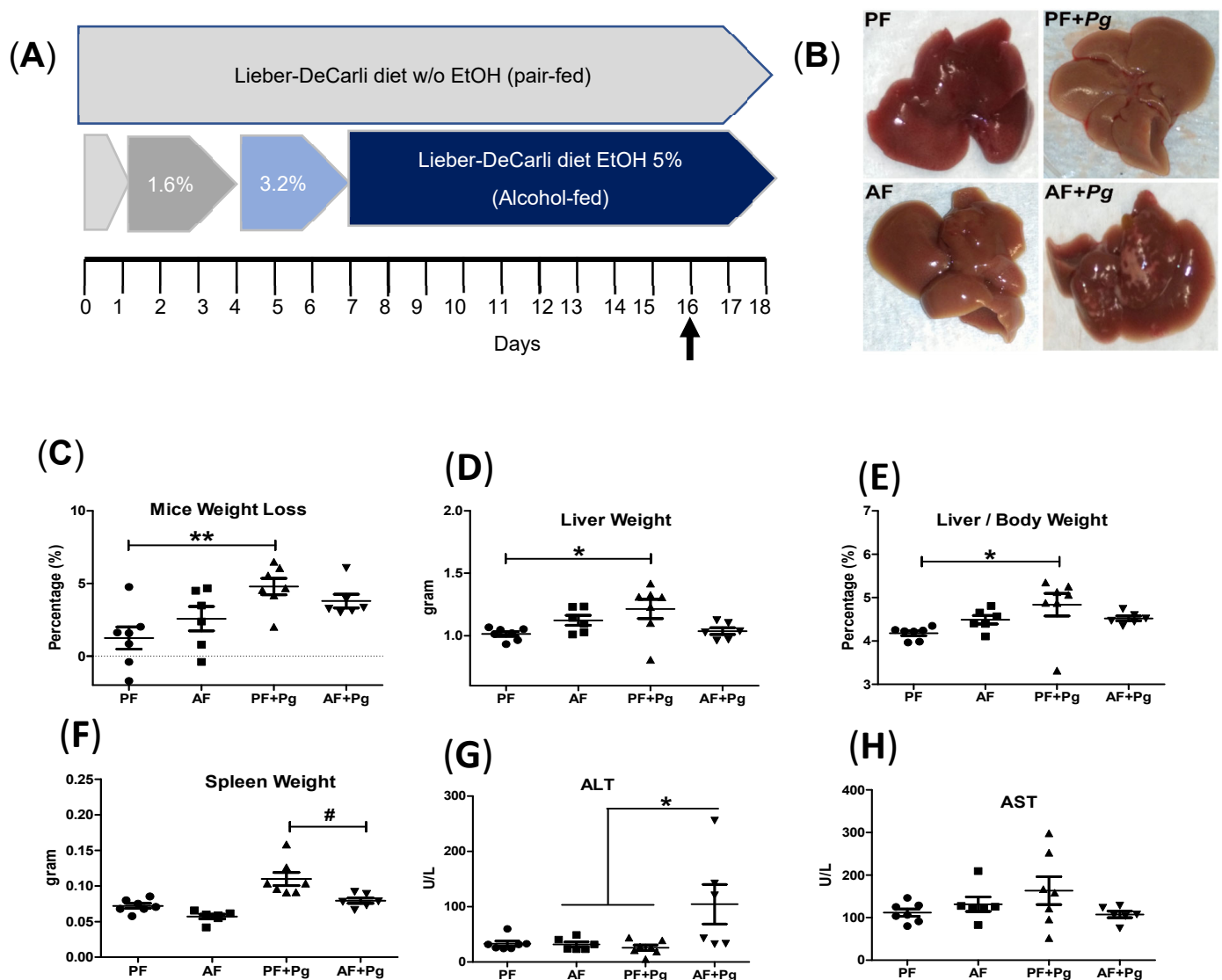


Figure 1. *Pg* infection of alcohol-fed mice induced liver injury. (A) Experimental diagram. Mice fed with the Lieber–DeCarli liquid diet with/without ethanol (EtOH) for total of 18 days; mice infected with *Pg* on day 16 (shown by arrow) and sacrificed on day 18. (B) Representative images of livers. (C–E) mice weight loss, liver weights and liver/body weight ratios. (F) Mice spleen weights. (G) Serum ALT values. (H) Serum AST values. Data are expressed as mean \pm SEM ($n = 6$ –7). One-way ANOVA with Tukey’s post-hoc test (marked as *) or Two-tailed unpaired t test (marked as #) (* or # $p < 0.05$; ** $p < 0.01$).

2.3. RNA Isolation and Real-Time Polymerase Chain Reaction (Real-Time PCR)

Liver tissues were homogenized by sonication, and total RNA was isolated using Trizol according to the manufacturer’s protocol (Invitrogen, Carlsbad, CA, USA). High-Capacity cDNA Reverse Transcription Kit (ThermoFisher, Waltham, MA, USA) was used for cDNA reverse-transcription as follows: according to the manufacture protocol, a 20- μ L reaction system was composed of 2 μ L 10 \times RT Buffer, 2 μ L 10 \times RT Random Primers, 0.8 μ L 25 \times dNTP Mix (100 mM), 1 μ L MultiScribe™ Reverse Transcriptas (50 U/ μ L), and 14.2 μ L Nuclease-free H₂O with 2 μ g of total liver RNA; the reaction cycle included 25 $^{\circ}$ C for 10 min, 37 $^{\circ}$ C for 120 min, 85 $^{\circ}$ C for 5 min and 4 $^{\circ}$ C for holding. PCR primers for universal bacteria and mouse 18S rRNA were obtained from previous studies [19,20], and other primers were

designed (Table 1). Real-time PCR was performed on ABI StepOnePlus™ Real-Time PCR System (ThermoFisher) with Power SYBR Green PCR Master Mix (ThermoFisher). Fold change in gene expression was calculated using the formula $2^{-\Delta\Delta C_t}$. Dissociation curve analysis was performed after PCR amplification to confirm the specificity of the primers. Gene expression was normalized to the housekeeping gene, β -actin (*Actb*). For comparisons of clearance of *P. gingivalis* and other bacterial infections, *16S rRNA* of *P. gingivalis* and universal bacteria were normalized to mouse *18S rRNA*.

Table 1. Primers used in current study.

Gene Name	Forward Primer (FW)	Reverse Primer (RE)
<i>Actb</i>	5'-AGACTTCGAGCAGGAGATGG	5'-CGCTCGTTGCCAATAGTGAT
<i>Ccr2</i>	5'-GCCTGATCCTGCCTTACTT	5'-GGCAAAGATGAGCCTCACAG
<i>Ccr5</i>	5'-CACACCCTGTTTCGCTGTAG	5'-ATTCTTGGAAAGGTGGTCAGG
<i>Ccl2</i>	5'-GGCCTGCTGTTCACAGTTGC	5'-CCTGCTGCTGGTGATCCTCT
<i>Myd88</i>	5'-CAAGTTTGCACCTCAGCCTGT	5'-AACCGCAGGATACTGGGAAA
<i>Il6</i>	5'-TCCAGTTGCCTTCTTGGGACT	5'-GCCTCCGACTTGTGAAGTGGT
<i>Tnf</i>	5'-CCAGCCGATGGGTTGTACCT	5'-TGACGGCAGAGAGGAGGTTG
<i>Il1b</i>	5'-GGCCTTGGGCCTCAAAGGAA	5'-GCTTGGGATCCACACTCTCCA
<i>Ifng</i>	5'-CAGGCCATCAGCAACAACAT	5'-GACCTGTGGGTGTTGACCT
<i>Ncf1</i>	5'-CTTCAGACCTATCGGGCCAT	5'-CGCTTTGTCTTCATCTGGCA
<i>Lcn2</i>	5'-ATGTCACCTCCATCCTGGTC	5'-GTGGCCACTTGCACATTGTA
<i>C5ar1</i>	5'-TCCTGCTGCTGGCTACCATT	5'-GCTAAGACCCAGGCCACTCC
<i>Cybb</i>	5'-TTGCTGTGCACCATGATGAG	5'-GGGTGTTCACTTGCAATGGT
<i>Sod2</i>	5'-CCGAGGAGAAGTACCACGAG	5'-TAGGGCTCAGGTTTGTCCAG
<i>Cd18</i>	5'-GCCCTCAACGAGATCACCGA	5'-CTGGCAGGCCTTCTCCTTGT
<i>Pg 16S rRNA</i>	5'-CTGACACTGAAGCACGAAGG	5'-CTTAACGCTTTCGCTGTGGA
<i>Universal 16S</i>	5'-ACTCCTACGGGAGGCAGCAGT	5'-ATTACC GCGGCTGCTGGC
<i>18S rRNA</i>	5'-CCGACACGGACAGGATTGA	5'-GCATGCCAGAGTCTCGTTCCG
<i>C5ar2</i>	5'-CCTGGCTCACAGTGCTCTCA	5'-TGGTCCACCGCACTTTCCTCA
<i>Tlr9</i>	5'-AGCCTGAGCCACCAACAT	5'-GTCACCTTACCGCTCCTGT
<i>Il18</i>	5'-TTTCTGGACTCCTGCCTGCT	5'-TGGAAGGTTTGTAGGCGGCTT
<i>Hmgb1</i>	5'-AATCAAAGGCGAGCATCCTG	5'-TCAGCTTGGCAGCTTCTTC
<i>Tgfb1</i>	5'-CCCCTGGCTTCTAGTGCTGA	5'-ACAGGATCTGGCCACGGATG
<i>ChREBP</i>	5'-GACAGCGGAGTACATCCTGA	5'-AAGTTGATGGCAGCGTTGAG
<i>Srebf1</i>	5'-GCAAGGCCATCGACTACATC	5'-CTGACACCAGGTCCTTCACT
<i>Fasn</i>	5'-AAGTTGCCCGAGTCAGAGAA	5'-TTCCAGACCGCTTGGGTAAT

2.4. Western Blot Analysis, Serum Lcn2 ELISA Assay and Serum AST/ALT Activity Measurement

Hepatic tissues were lysed with cold cell lysis buffer containing phosphatase inhibitor and protease inhibitor and centrifuged for 15 min at $12,000 \times g$ at $4^\circ C$. The protein concentration was measured using a BCA assay kit (Pierce, Rockford, IL, USA). Proteins (50 μg) were separated by SDS-PAGE, blotted onto a polyvinylidene difluoride membrane (PVDF), and blocked with 5% bovine serum albumin in Tris-buffered saline with 0.1% Tween 20. Blots were reacted for 16 h with primary antibody Lipocalin-2/NGAL (R&D systems, Minneapolis, MN, USA) at $4^\circ C$ for 1 h with the secondary antibody (Abcam, Boston, MA, USA) at room temperature. The membrane was developed by using Luminata™ Western horseradish peroxidase (HRP) substrate (ThermoFisher). β -actin (Sigma, St. Louis, MO) was used as a loading control. Mouse serum Lcn2 was measured by using Lipocalin-2 (Lcn2) ELISA Kit (ThermoFisher). Serum alanine aminotransferase (ALT) assay and aspar-

tate aminotransferase (AST) were performed by using ALT (ThermoFisher) and AST assay kit (Fisher Sci. Waltham, MA, USA) according to the manufacturer's instructions.

2.5. Immunohistochemistry Staining

Liver frozen tissue were sectioned at 5 μm thickness. Slides were washed with PBS and fixed with 4% PFA at RT for 10 min. After permeabilization, slides were blocked with 5% goat serum for 1 h at RT and incubated with primary antibody anti-F4/80 (Abcam 1:100 dilution) overnight. After washing with TBST (0.1%) 4 times for 5 min each, a secondary antibody (Alexa Fluor 555 labeled donkey anti-rat IgG, Abcam, 1:1000 dilution) was applied for 1 h at room temperature. After washing with TBST (0.1%) for 4 \times 5 min, slides were mounted with antifade mounting media (Vector Laboratories, Newark, CA, USA) and pictures were taken under a fluorescent microscope.

2.6. Liver Tissue Hematoxylin and Eosin Staining (H&E Staining) [21]

Paraffin-embedding live tissue were sectioned at 6 μm thickness. After deparaffinization and re-hydration, slides were stained with hematoxylin for 1 min. After washing for 10 min in tap water, slides were stained with eosin for 30 s to 1 min. After dehydration, slides were mounted at Permount medium (Fisher Sci.) and covered with coverslips.

2.7. Naphthol AS-D Chloroacetate Esterase (CAE) Staining

Neutrophil infiltration was detected by using chloroacetate esterase (CAE) staining (Sigma) according to manufacturer's instructions. Deparaffinized tissue slides were fixed for 1 min in citrate-acetone-methanol fixative at room temperature, washed thoroughly in deionized water and air dried for at least 20 min. Then slides were stained with pre-warmed staining solution (37 $^{\circ}\text{C}$) (50 mL TRIZMAL with 1 capsule Fast Corinth V Salt plus 2 mL CAE solution) for 15 min. Slides were washed in deionized water for 3 min and counterstained in acid hematoxylin solution for 1 min. Slides were mounted with an aqueous mounting media after being washed in tap water for 10 min.

2.8. Terminal Deoxynucleotidyl Transferase dUTP Nick End Labeling (TUNEL) Assay

Cell death was analyzed by using apoptag peroxidase in situ apoptosis detection kit (Chemicon, Temecula, CA, USA) according to manufacturer's instructions. Liver cryosections were fixed in 1% paraformaldehyde in PBS (pH 7.4) for 10 min at RT. After washing with PBS twice for 5 min each, slides were post-fixed in precooled ethanol: acetic acid (2:1) for 5 min at -20°C . After draining and washing twice in PBS, slides were quenched in 3% hydrogen peroxide in PBS for 5 min at RT. After being rinsed twice with PBS or dH_2O (5 min each time), equilibration buffer was applied for at least 10 s at RT. Following this, slides were incubated with working strength TdT enzyme in a humidified chamber at 37 $^{\circ}\text{C}$ for 1 h and then with stop/wash buffer for 10 min at RT. After 3 times washing with PBS (each wash for 1 min), slides were incubated with anti-digoxigenin peroxidase conjugated at room temperature in a humidified chamber for 30 min. After 4 wash cycles (2 min each wash), slides were incubated with TMB (Fisher Sci) for 3 to 6 min at room temperature. After 3 times washing in dH_2O (1 min each wash), slides were counterstained in hematoxylin working solution for 1 min and washed for 10 min in ddH_2O . Images were taken, and data were analyzed.

2.9. Statistical Analysis

Due to mortality during alcohol feeding and *Pg* challenging, two mice died in the alcohol feeding group; two mice died after *Pg* infection in AF+*Pg* group. Accordingly, 6–7 mice in each group were used to perform statistical analysis at the experimental end. GraphPad Prism software 5.04 (GraphPad Software Inc., San Diego, CA, USA) was used for data analyses. Data were expressed as mean \pm SEM and analyzed by one-way analysis of variance (ANOVA) with Tukey's *post-hoc* correction (marked as *), or unpaired *t* tests

(marked as #) where appropriate. Differences were considered statistically significant when $p < 0.05$.

3. Results

3.1. *Pg* Infection of Alcohol-Fed Mice Induced Liver Injury

Mice were fed a liquid diet containing alcohol (AF) or a pair-fed isocaloric control diet (PF) (Figure 1A). Two days before sacrifice, mice were injected with *Pg*. *Pg* infection in PF mice resulted in a significant reduction in body weight but increased liver weight (Figure 1C–E). Liver staining revealed pale appearances in *Pg*-challenged PF mice (PF+*Pg* mice) (Figure 1B). In contrast, AF+*Pg* mice exhibited purulent infections with noticeable liver abscess lesions (Figure 1B) and a significant reduction in spleen weight compared to PF+*Pg* mice (Figure 1F). Serum ALT levels were significantly elevated in AF+*Pg* mice compared to PF+*Pg* and AF mice (Figure 1G,H). These results suggest that immune system mobilization in PF+*Pg* mice helped combat *Pg* infection effectively both in spleen and liver, whereas AF+*Pg* mice experienced liver injuries and dysfunction of immune response due to systemic immunosuppression.

3.2. *Pg* Infection of Alcohol-Fed Mice Induced Infiltration of Inflammatory Monocytes/Macrophages but Repressed Expression of Inflammatory Cytokines

The mRNA levels of CC chemokine receptors 2 and 5 (*Ccr2* and *Ccr5*) involved in liver inflammation and macrophage recruitment were significantly upregulated in AF+*Pg* mice, compared to AF and PF+*Pg* mice, while gene expression level of the ligand *Ccl2* was not changed (Figure 2A–C). AF+*Pg* mice exhibited downregulated mRNA expression levels of the Tlr adaptor *Myd88*, as well as the inflammatory cytokines *Tnf*, *Il1b*, and interferon γ (*Ifng*) compared to PF+*Pg* mice; in contrast, compared to all other groups, gene expression level of *Tnf* was significantly upregulated in AF mice (Figure 2D,F–H). Interestingly, *Pg* infection significantly suppressed *Il6* expression, while there was increased *Ifng* expression in both *Pg* infection of PF and AF mice; by contrast, compared to PF+*Pg* mice, the expression level of *Ifng*, not *Il6* was significantly downregulated in AF+*Pg* mice (Figure 2E,H). Liver tissue analysis showed the presence of inflammatory monocyte/macrophage infiltration and defective migration of inflammatory monocytes/macrophages in AF+*Pg* mice, as indicated by piled-up F4/80-positive cells in the liver tissue (Figure 2I).

3.3. *Pg* Infection of Alcohol-Fed Mice Induced Neutrophil Infiltration and Defective Bacterial Clearance

The mRNA levels of hepatic neutrophil cytosol factor 1 (*Ncf1*) and complement component C5a receptor *C5ar1* were significantly upregulated in AF+*Pg* mice compared to AF and PF+*Pg* mice (Figure 3A,B). The neutrophilic inflammation driver lipocalin 2 (*Lcn2*) mRNA level was elevated by *Pg* infection in both PF and AF mice; and, compared to all other groups, gene expression level of *Lcn2* was significantly upregulated in AF+*Pg* mice (Figure 3C). *Sod2* mRNA expression level was not affected by alcohol feeding or *Pg* infection in PF mice, but significantly increased by *Pg* infection in AF mice compared to the PF+*Pg* mice (Figure 3D). The mRNA expression levels of NADPH oxidase 2 (*Cybb*) and complement receptor 3 (*Cr3*) component/ the leukocyte adhesion molecule *Cd18* were significantly increased in *Pg* infection of both PF and AF mice but decreased in AF+*Pg* mice compared to PF+*Pg* (Figure 3E,F). *Pg* 16S rRNA and universal 16S rRNA expression levels were significantly upregulated in AF+*Pg* mouse livers compared to PF+*Pg* mice, indicating impaired bacterial (including *Pg* and other bacteria) clearances in livers of AF+*Pg* mice (Figure 3G,H). Immuno-blot analysis demonstrated elevated *Lcn2* protein levels in *Pg*-infected mice (both AF and PF) and, compared to PF+*Pg* mice, stronger bands of *Lcn2* in AF+*Pg* mice (Figure 3I). Serum *Lcn2* levels were significantly increased in *Pg*-infected mice (Figure 3J). Liver staining showed prominent intrahepatic neutrophil infiltration in AF+*Pg* mice and hypertrophic hepatocytes in PF+*Pg* mice (Figure 3K). These findings indicate increased intrahepatic neutrophil infiltration and defective clearance of *Pg* in AF+*Pg* mice, leading to neutrophilic inflammation and overt infections in liver.

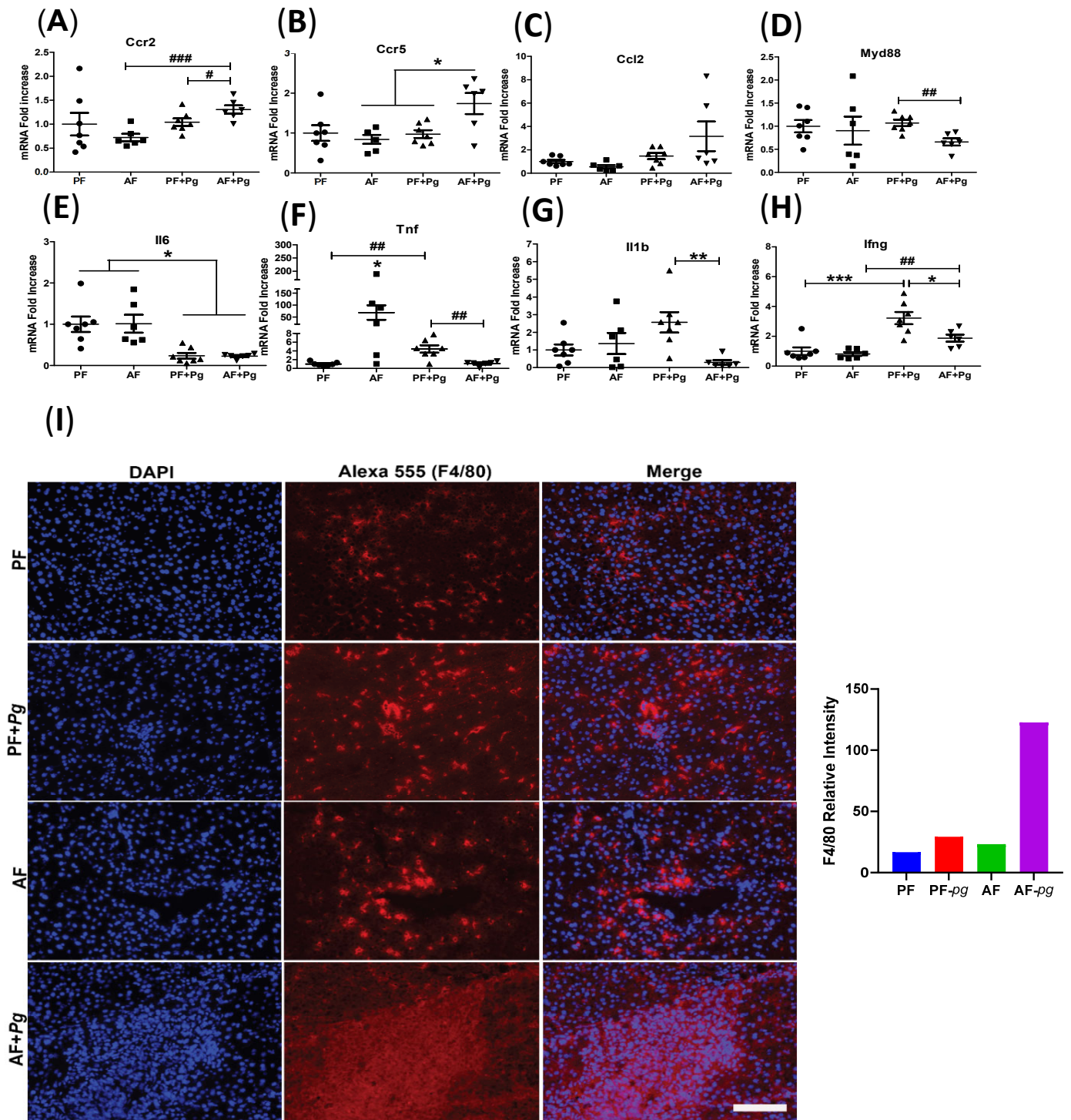


Figure 2. *Pg* infection of alcohol-fed mice induced liver infiltration of inflammatory monocytes/macrophages and repressed inflammatory cytokine expression in mice livers. (A–H) Relative gene mRNA expression levels in the livers. (I) Representative liver F4/80 macrophage staining; white scale bar is 100 μ m. Data are expressed as mean \pm SEM ($n = 6$ –7). Groups differ significantly (* or # $p < 0.05$; ** or ## $p < 0.01$; *** or ### $p < 0.001$).

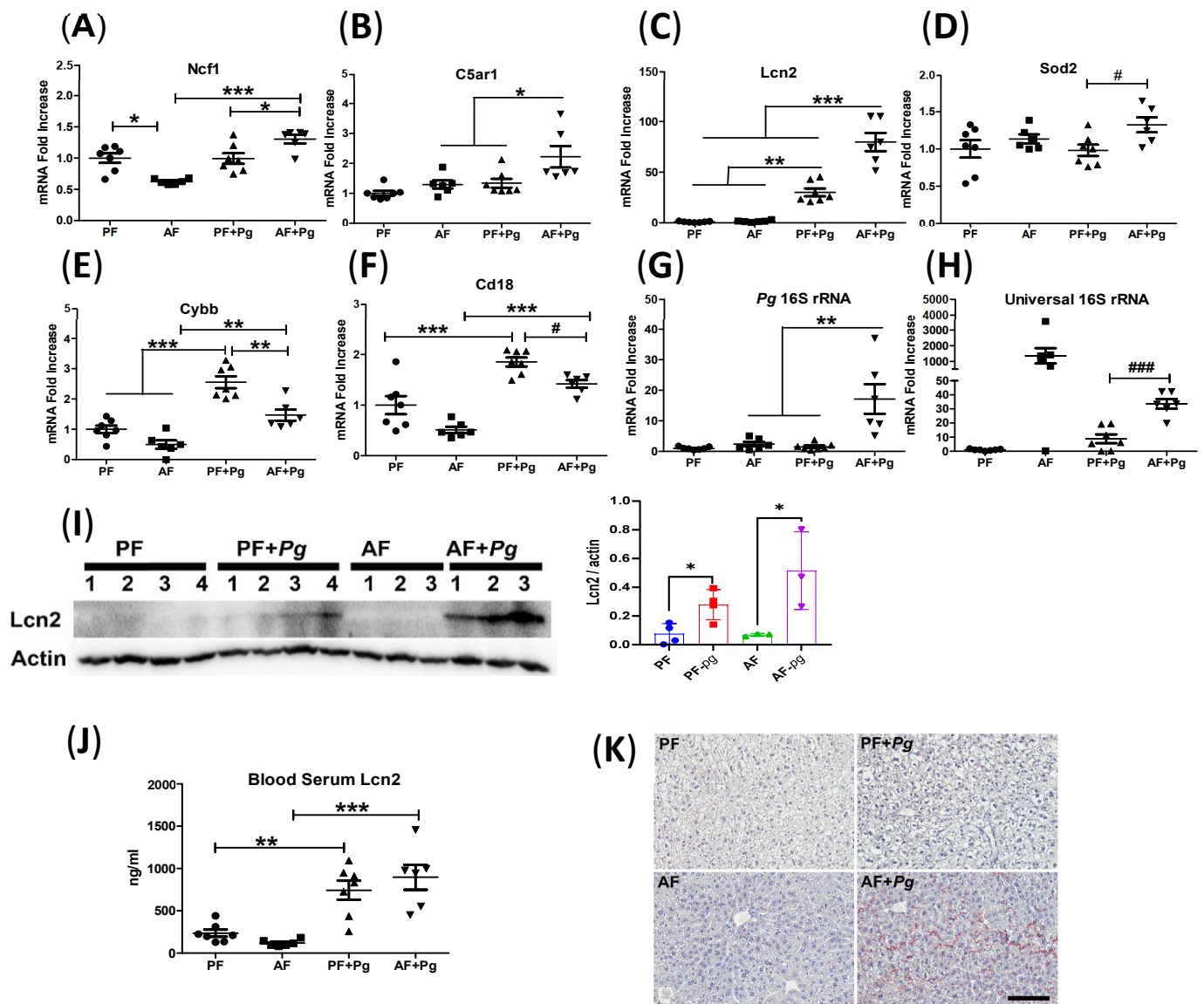


Figure 3. *Pg* infection of alcohol-fed mice induced neutrophil infiltration to liver and defective clearance of *Pg* and infections in mice livers. (A–F) Relative liver gene mRNA expression levels. (G,H) Relative liver *Pg* and universal 16S rRNA levels. (I) Immuno-blot analysis of Lcn2 in the livers. (J) Serum Lcn2 protein levels. (K) Representative liver CAE staining; pictures were taken under 20× magnification power, black scale bar is 100 μm. Data are expressed as mean ± SEM ($n = 6-7$). Groups differ significantly (* or # $p < 0.05$; ** $p < 0.01$; *** or ### $p < 0.001$).

3.4. *Pg* Infection of Alcohol-Fed Mice Induced Inflammasome Activation and Cell Death

The mRNA levels of inflammasome-related genes, including complement component C5a receptor *C5ar2*, toll-like receptor 9 (*Tlr9*), interleukin-18 (*Il18*), and high mobility group box 1 (*Hmgb1*), were significantly upregulated in AF+Pg mice compared to PF+Pg mice. Alcohol feeding significantly increased the mRNA expression of *Tlr9*, but not *C5ar2*, *Il18*, and *Hmgb1* (Figure 4A–D). In contrast, the mRNA level of the efferocytosis-related gene *Tgfb1* tended to be significantly decreased in PF and AF+Pg mice compared to PF+Pg mice (Figure 4E). Liver histology revealed liver injury with necrotic cell death and increased eosinophilia staining in AF+Pg mice (Figure 4F). TUNEL staining demonstrated prominent apoptotic cell death in PF+Pg mice, whereas AF+Pg mice showed pyroptotic cell death with TUNEL-positive staining [22] (Figure 4G). These results indicate that *Pg* infection in PF mice induced apoptotic cell death, while in AF mice, in addition to apoptotic cell death,

Pg infection activated inflammasome and led to inflammation-associated necrotic cell death in liver [23].

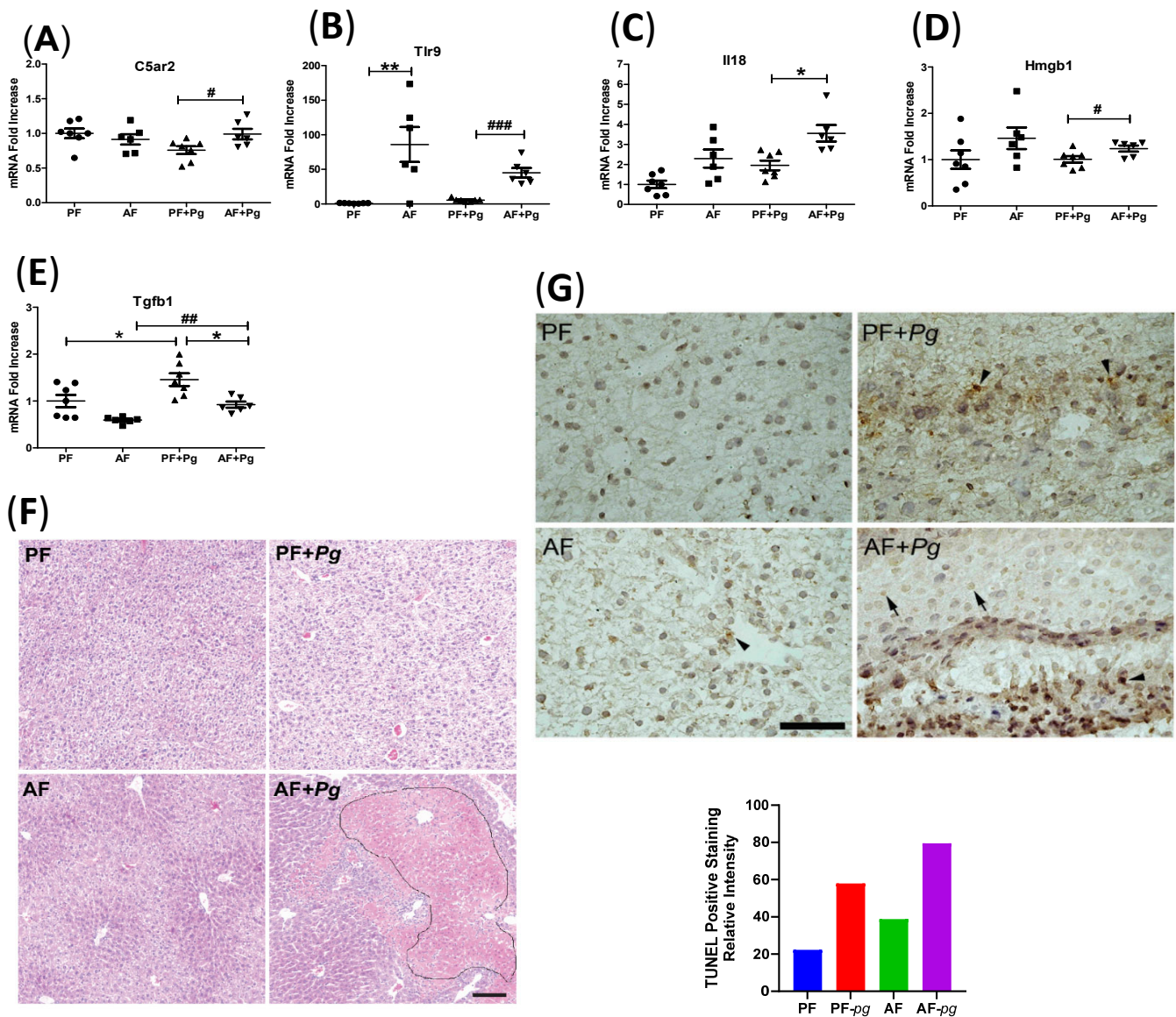


Figure 4. *Pg* infection of alcohol-fed mice induced inflammasome activation and cell death in mice livers. (A–E) Relative liver gene mRNA expression levels. (F) Representative liver H and E staining showing necrotic cell death with increased eosinophilia staining in AF+*Pg* mice (circle line); pictures were taken under 10× magnification power, black scale bar is 100 μm. (G) Representative liver TUNEL staining showing TUNEL-positive apoptosis (arrowheads) and TUNEL-positive pyroptotic cells at a lower staining intensity (arrows); pictures were taken under 40 × magnification power, black scale bar is 50 μm. Data are expressed as mean ± SEM ($n = 6-7$). Groups differ significantly (* or # $p < 0.05$, ** or ## $p < 0.01$, ### $p < 0.001$).

3.5. *Pg* Infection of Alcohol-Fed Mice Induced Lipogenesis-Related Gene Expression

Alcohol feeding increased liver steatosis, and the mRNA expression of lipogenic genes *Srebf1* and *Fasn* was upregulated. However, *Pg* infection induced only minimal elevation in these genes (Figure 5A,B). The mRNA level of *ChREBP*, another major lipogenic gene, remained unchanged between PF and AF mice but was significantly increased only in AF+*Pg* mice (Figure 5C). These findings suggest that alcohol feeding primarily contributes to increased lipogenesis in *Pg*-infected AF mice livers.

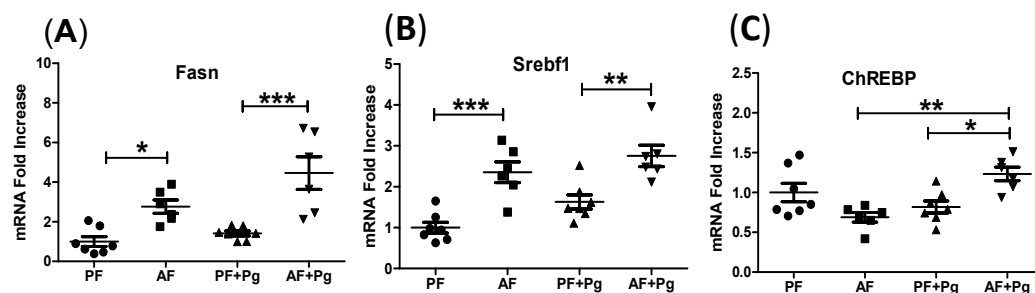


Figure 5. *Pg* infection of alcohol-fed mice induced lipogenesis-related gene expression in mice livers. (A–C) Relative liver gene mRNA expression levels. Data are expressed as mean \pm SEM ($n = 6$ –7). Groups differ significantly (* $p < 0.05$, ** $p < 0.01$, *** $p < 0.001$).

4. Discussion

Our previous findings have demonstrated a correlation between levels of circulating antibodies against *Pg* and the severity of alcoholic hepatitis (AH) in patients [14]. The association between periodontitis and liver diseases is supported by growing evidence [24], although the exact nature of this relationship remains unclear. To address this, we conducted the present study to investigate whether systemic challenge with *Pg*, one of the major pathogens associated with periodontitis, contributes to the development of ALD in mice.

Several models have been utilized to study ALD in mice. Among these, the chronic plus binge model has gained significant popularity in recent years [18,25]. In this model, mice are subjected to a 10 day to 8 week regimen of a 5% EtOH-containing liquid diet, followed by a binge dose of EtOH administered shortly before sacrificing the animals. This model has demonstrated that chronic EtOH consumption sensitizes the liver, making it more susceptible to subsequent challenges, either from alcohol or other “second” insults, resulting in an exacerbated inflammatory response. It mimics ALD well, which is characterized by steatosis and liver inflammation. In the current study, we aimed to investigate whether *Pg* infection could serve as a “second hit” in this context.

Our mouse model holds relevance because patients with periodontitis are believed to experience non-symptomatic bacteremia. Although the IP route of *Pg* inoculation does not directly reflect the natural oral habitat of *Pg*, it does simulate the reaching of the liver for *Pg* through the bloodstream following bacteremia in patients associated with periodontitis. Therefore, we hypothesized that this systemic bacterial infection, in conjunction with ethanol exposure, would synergistically promote the development of ALD.

Sepsis is a common complication in patients with ALD [26]. Previous studies have reported that subcutaneous injection of *Pg* at a dose of 1×10^9 CFU/mouse can induce abscess formation in the inguinal area [27]. In our current study, a lower dose of 2×10^8 CFU/animal of *Pg* administered via IP injection to pair-fed (PF) mice resulted in significant increases in liver weights and decreases in body weights. These changes, along with hepatocyte hypertrophy, indicate that PF mice were able to mount an active response to the infection [15,28]. In contrast, alcohol-fed (AF) mice challenged with *Pg* exhibited reduced spleen weights, elevated serum ALT levels, and noticeable abscess lesions in the liver, suggesting liver immune suppression [29,30], immune cell infiltration, and liver injury, as decreased spleen weights in AF+*Pg* mice indicated that splenic macrophages were likely to be unable to be activated for the removal of bacteria from the blood during systemic infections [31]. The presence of pus, which consists of white blood cells and dead cells and is formed during the body’s defense against bacterial infection [23], further supports the notion of both systemic and liver immune suppression. Therefore, *Pg* infection complicates alcohol-associated liver injury.

We further explored the mechanisms underlying *P. gingivalis*-induced ALD in our mouse model. We observed recruitment of Ccr2+ inflammatory monocytes to the liver in AF+*Pg* mice, as evidenced by upregulated gene expression levels of *Ccr2* and *Ccr5*, as well

as F4/80 macrophage staining. *Ccr2* and *Ccr5* are predominantly expressed on the surface of inflammatory monocytes/macrophages [32,33]. Upregulated gene expression levels of *Tnf* in AF mice indicate that alcohol can activate resident liver macrophages, known as Kupffer cells (KC) [34]. However, this activation is suppressed in AF mice infected with *Pg*, as demonstrated by downregulated gene expression levels of *Myd88* [35], *Tnf*, *Il1b*, and *Infg* [36]. Furthermore, compared to PF+*Pg* mice, AF+*Pg* mice showed upregulated gene expression levels of complement 5a receptors *C5ar1/C5ar2*, indicating the activation of *C5ar-Tlr2* crosstalk signaling, and downregulated complement receptor *Cr3* (*Cd11b/Cd18*) in the macrophage lineage, which could contribute to immune response suppression with downregulated gene expression levels of cytokines [9,37].

Additionally, intrahepatic neutrophil infiltration and neutrophilic inflammation were confirmed in AF+*Pg* mice, as indicated by elevated gene expression levels of neutrophil cytosol factor 1 (*Ncf1*), neutrophilic inflammation driver *Lcn2*, and positive liver CAE staining [1,30]. We demonstrated that, after 2 days of *Pg* infection, liver injuries were driven by intrahepatic neutrophils in AF+*Pg* mice, as evidenced by the upregulated gene expression level of *Ncf1* [1,38]. Comparing AF+*Pg* mice to PF+*Pg* mice, upregulated gene expression levels of *Lcn2*, *C5ar1*, and *C5ar2* indicate that neutrophils could be recruited by “intermediate-target” signal *Lcn2* [39] and “end-target” molecule C5a [40]. Alcohol feeding-induced oxidized C5, converted by gingipains of *Pg*, is known to activate neutrophils and promote their activation, including polarization, chemotaxis, and exocytosis. Thus, *Pg* challenge induces hepatocytes to secrete *Lcn2* [41], mobilizing neutrophils to the liver, and the presence of neutrophils in the liver parenchyma, i.e., intrahepatic neutrophil infiltration, is further guided by upregulated *Lcn2* and oxidized C5 converted by gingipains.

We found that the neutrophil function of bacterial killing was compromised in AF+*Pg* mice, as *Pg* infection subverted the major neutrophil functions [42]. Upregulated *Pg* 16S *rRNA* and universal 16S *rRNA* in *Pg*-challenged AF mice indicate that the livers were unable to effectively clear the *Pg* infection and bacterial translocation from the intestine. This finding is further supported by the downregulation of gene expression levels of *Myd88*, *Tnf*, *Infg*, and *Cybb* in AF+*Pg* mice. *Myd88* is a Toll-like receptor (TLR) adaptor protein [35], *Tnf* and *Infg* are neutrophil priming factors [43,44], and *Cybb* mediates neutrophil NADPH oxidase 2 oxidative killing [45]. Furthermore, neutrophils use two $\beta 2$ integrins, *Lfa-1* (*Cd11a/Cd18*) and *Mac-1* (*Cd11b/Cd18*), to mediate firm adhesion to activated endothelium [46]. Under the conditions of *Pg* infection in AF mice, downregulated gene expression level of *Cd18* [47] could impair the clearance of infection, as *Cd18* is a leukocyte adhesion molecule as well as a *Cr3* component involved in neutrophil migration, and complement C3-opsonized particle-mediated phagocytosis [48] and phagocytosis-induced cell death (PICD) [49]. Additionally, *Pg* infection of AF mice modified neutrophil apoptosis [50], as further evidenced by the upregulated gene expression levels of *Sod2* [51,52] and *Tlr9* [53], and downregulated *Cd18* [54] in AF+*Pg* mice. Meanwhile, neutrophil dysfunction may induce neutrophils to limit infections by secreting *Lcn2* for sequestering the iron-laden siderophore, and the upregulated *Lcn2* could drive further neutrophilic inflammation [30].

We further demonstrated that the inflammasome pathway could be activated in macrophages in AF+*Pg* mice [55] as, compared to PF+*Pg* mice, gene expression levels of *C5ar2*, *Il18* and *Hmgbl* were upregulated [56]. Extracellular mitochondrial DNA could promote NLRP3 inflammasome activation in macrophages through *Tlr9* [57]. *Hmgbl* and *P. gingivalis*-derived outer membrane vesicles (OMVs) could lead to inflammasome activation in macrophages, neutrophils, and hepatocytes [23]. Compared to PF+*Pg* mice, downregulated gene expression levels of *Tgfb1* in AF+*Pg* mice indicate inefficient efferocytosis by KCs/macrophages, as the ingestion of apoptotic cells promotes M2 macrophages to produce TGF- $\beta 1$ [58]. Downregulated *Cd18* in KCs/macrophages and gingipains [59,60] could inhibit their migration to target sites in order to induce neutrophil apoptosis, which could impair inflammation resolution. Consequently, inflammation-associated pyroptosis, necroptosis, and delayed resolution of inflammation could induce secondary necrosis in AF+*Pg* mice, further recruiting immune cells and contributing to liver injury.

Furthermore, *Pg* infection of AF mice played a role in inflammation-induced hepatic steatosis. Alcohol feeding induces liver steatosis in both AF and AF+*Pg* mice, as evidenced by the upregulation of *Fasn*, *Srebf1* and *ChREBP*. We also observed an upregulation of *Ncf1* in AF+*Pg* mice. *Ncf1* plays a role in immune cell infiltration that damages insulin receptor substrate 1 (IRS1) [61] in hepatocytes and stimulates *ChREBP* expression, leading to lipogenesis [34]. Collectively, *Pg* infection of alcohol-sensitized livers mediated the pathogenesis of alcoholic liver steatosis in AF+*Pg* mice, likely through the alcohol feeding-induced *Srebf1*/*Fasn* pathway and *Pg* infection of the AF-induced *ChREBP*/*Fasn* pathway [1,62,63].

In summary, the data suggest that systemic *Pg* infection exacerbates alcohol-induced liver injury and steatosis with dysfunction of immune response. Although further experimental study evaluating the role of *Pg* infection due to periodontal disease is needed to reveal the correlation between oral microbiome and ALD, the current study provided evidence that *Pg* can serve as the “second hit” in the development and progression of ALD.

Author Contributions: Y.Z. performed the experiments, analyzed data, and drafted and revised the manuscript; C.M. contributed to the critical discussion of the project and critical revision of the manuscript; W.F. conceived, designed, and supervised the study and drafted and critically revised the manuscript. All authors have read and agreed to the published version of the manuscript.

Funding: The current study was supported by National Institutes of Health grants R21AA022416, R01AA023190 (WF); 1U01AA026934-01, 1U01AA026936-01, 1U01AA026980-01 (CJM), 1I01BX002996-01A2 (CJM), and research reported in this publication was supported by an Institutional Development Award (IDeA) from the National Institute of General Medical Sciences of the National Institutes of Health under grant number P20GM113226 (CJM), and the National Institute on Alcohol Abuse and Alcoholism of the National Institutes of Health under Award Number P50AA024337 (CJM). The content is solely the responsibility of the authors and does not necessarily represent the official views of the National Institutes of Health.

Institutional Review Board Statement: The animal study protocol was approved by the Institutional Animal Care and use Committee of University of Louisville (protocol code 21977 approved on 2 December 2021).

Informed Consent Statement: Not applicable.

Data Availability Statement: No new data were created.

Acknowledgments: The authors are thankful to Marion McClain for manuscript proofreading.

Conflicts of Interest: The authors declare no conflicts of interest.

Abbreviations

AH	alcohol-associated steatohepatitis
AF	alcohol-fed
ALD	alcohol-associated liver diseases
ALT	alanine aminotransferase
AST	aspartate aminotransferase
<i>C5ar</i>	C5a receptor
<i>Cr3</i>	complement receptor 3
CFU	colony-forming units
H and E	hematoxylin and eosin
<i>Hmgb1</i>	high mobility group box-1 protein gene
IP	intraperitoneal injection
KC	Kupffer cell
<i>Lcn2</i>	lipocalin 2
<i>Ncf1</i>	Neutrophil cytosol factor 1
PBS	phosphate-buffered saline
PD	periodontal disease
<i>Pg</i>	<i>P. gingivalis</i> W83 stain infection
PF	pair-fed
TUNEL	terminal deoxynucleotidyl transferase dUTP nick end labeling assay

References

1. Ma, J.; Guillot, A.; Yang, Z.; Mackowiak, B.; Hwang, S.; Park, O.; Peiffer, B.J.; Ahmadi, A.R.; Melo, L.; Kusumanchi, P.; et al. Distinct histopathological phenotypes of severe alcoholic hepatitis suggest different mechanisms driving liver injury and failure. *J. Clin. Investig.* **2022**, *132*, e157780. [[CrossRef](#)]
2. Liangpunsakul, S.; Haber, P.; McCaughan, G.W. Alcoholic Liver Disease in Asia, Europe, and North America. *Gastroenterology* **2016**, *150*, 1786–1797. [[CrossRef](#)]
3. Asrani, S.K.; Mellinger, J.; Arab, J.P.; Shah, V.H. Reducing the Global Burden of Alcohol-Associated Liver Disease: A Blueprint for Action. *Hepatology* **2021**, *73*, 2039–2050. [[CrossRef](#)]
4. Younossi, Z.M.; Stepanova, M.; Younossi, Y.; Golabi, P.; Mishra, A.; Rafiq, N.; Henry, L. Epidemiology of chronic liver diseases in the USA in the past three decades. *Gut* **2020**, *69*, 564–568. [[CrossRef](#)]
5. Novacek, G.; Plachetzky, U.; Potzi, R.; Lentner, S.; Slavicek, R.; Gangl, A.; Ferenci, P. Dental and periodontal disease in patients with cirrhosis—Role of etiology of liver disease. *J. Hepatol.* **1995**, *22*, 576–582. [[CrossRef](#)]
6. Day, C.P.; James, O.F. Steatohepatitis: A tale of two “hits”? *Gastroenterology* **1998**, *114*, 842–845. [[CrossRef](#)]
7. Lunar Silva, I.; Cascales, E. Molecular Strategies Underlying *Porphyromonas gingivalis* Virulence. *J. Mol. Biol.* **2021**, *433*, 166836. [[CrossRef](#)]
8. Aleksijevic, L.H.; Aleksijevic, M.; Skrlec, I.; Sram, M.; Sram, M.; Talapko, J. *Porphyromonas gingivalis* Virulence Factors and Clinical Significance in Periodontal Disease and Coronary Artery Diseases. *Pathogens* **2022**, *11*, 1173. [[CrossRef](#)]
9. Hussain, M.; Stover, C.M.; Dupont, A.P. *gingivalis* in Periodontal Disease and Atherosclerosis—Scenes of Action for Antimicrobial Peptides and Complement. *Front. Immunol.* **2015**, *6*, 45. [[CrossRef](#)]
10. Maekawa, T.; Krauss, J.L.; Abe, T.; Jotwani, R.; Triantafilou, M.; Triantafilou, K.; Hashim, A.; Hoch, S.; Curtis, M.A.; Nussbaum, G.; et al. *Porphyromonas gingivalis* manipulates complement and TLR signaling to uncouple bacterial clearance from inflammation and promote dysbiosis. *Cell Host Microbe* **2014**, *15*, 768–778. [[CrossRef](#)]
11. Ruan, Q.; Guan, P.; Qi, W.; Li, J.; Xi, M.; Xiao, L.; Zhong, S.; Ma, D.; Ni, J. *Porphyromonas gingivalis* regulates atherosclerosis through an immune pathway. *Front. Immunol.* **2023**, *14*, 1103592. [[CrossRef](#)]
12. Zhou, N.; Zou, F.; Cheng, X.; Huang, Y.; Zou, H.; Niu, Q.; Qiu, Y.; Shan, F.; Luo, A.; Teng, W.; et al. *Porphyromonas gingivalis* induces periodontitis, causes immune imbalance, and promotes rheumatoid arthritis. *J. Leukoc. Biol.* **2021**, *110*, 461–473. [[CrossRef](#)]
13. Ahmadi, P.; Mahmoudi, M.; Kheder, R.K.; Faraj, T.A.; Mollazadeh, S.; Abdulabbas, H.S.; Esmaili, S.A. Impacts of *Porphyromonas gingivalis* periodontitis on rheumatoid arthritis autoimmunity. *Int. Immunopharmacol.* **2023**, *118*, 109936. [[CrossRef](#)]
14. Zhou, Y.; Vatsalya, V.; Gobejishvili, L.; Lamont, R.J.; McClain, C.J.; Feng, W. *Porphyromonas gingivalis* as a Possible Risk Factor in the Development/Severity of Acute Alcoholic Hepatitis. *Hepatol. Commun.* **2019**, *3*, 293–304. [[CrossRef](#)]
15. Naito, M.; Hirakawa, H.; Yamashita, A.; Ohara, N.; Shoji, M.; Yukitake, H.; Nakayama, K.; Toh, H.; Yoshimura, F.; Kuhara, S.; et al. Determination of the genome sequence of *Porphyromonas gingivalis* strain ATCC 33277 and genomic comparison with strain W83 revealed extensive genome rearrangements in *P. gingivalis*. *DNA Res.* **2008**, *15*, 215–225. [[CrossRef](#)]
16. Igboin, C.O.; Griffen, A.L.; Leys, E.J. *Porphyromonas gingivalis* strain diversity. *J. Clin. Microbiol.* **2009**, *47*, 3073–3081. [[CrossRef](#)]
17. Jiang, M.; Li, F.; Liu, Y.; Gu, Z.; Zhang, L.; Lee, J.; He, L.; Vatsalya, V.; Zhang, H.G.; Deng, Z.; et al. Probiotic-derived nanoparticles inhibit ALD through intestinal miR194 suppression and subsequent FXR activation. *Hepatology* **2023**, *77*, 1164–1180. [[CrossRef](#)]
18. Bertola, A.; Mathews, S.; Ki, S.H.; Wang, H.; Gao, B. Mouse model of chronic and binge ethanol feeding (the NIAAA model). *Nat. Protoc.* **2013**, *8*, 627–637. [[CrossRef](#)]
19. Clifford, R.J.; Milillo, M.; Prestwood, J.; Quintero, R.; Zurawski, D.V.; Kwak, Y.I.; Waterman, P.E.; Lesho, E.P.; Mc Gann, P. Detection of bacterial 16S rRNA and identification of four clinically important bacteria by real-time PCR. *PLoS ONE* **2012**, *7*, e48558. [[CrossRef](#)]
20. Gravitte, A.; Kintner, J.; Brown, S.; Cobble, A.; Kennard, B.; Hall, J.V. The hormonal environment and estrogen receptor signaling alters *Chlamydia muridarum* infection in vivo. *Front. Cell. Infect. Microbiol.* **2022**, *12*, 939944. [[CrossRef](#)]
21. Cardiff, R.D.; Miller, C.H.; Munn, R.J. Manual hematoxylin and eosin staining of mouse tissue sections. *Cold Spring Harb. Protoc.* **2014**, *2014*, 655–658. [[CrossRef](#)]
22. Jorgensen, I.; Miao, E.A. Pyroptotic cell death defends against intracellular pathogens. *Immunol. Rev.* **2015**, *265*, 130–142. [[CrossRef](#)]
23. Frank, D.; Vince, J.E. Pyroptosis versus necroptosis: Similarities, differences, and crosstalk. *Cell Death Differ.* **2019**, *26*, 99–114. [[CrossRef](#)]
24. Albuquerque-Souza, E.; Sahingur, S.E. Periodontitis, chronic liver diseases, and the emerging oral-gut-liver axis. *Periodontol.* **2000** *2022*, *89*, 125–141. [[CrossRef](#)]
25. Gao, B.; Xu, M.J.; Bertola, A.; Wang, H.; Zhou, Z.; Liangpunsakul, S. Animal Models of Alcoholic Liver Disease: Pathogenesis and Clinical Relevance. *Gene Expr.* **2017**, *17*, 173–186. [[CrossRef](#)]
26. Gustot, T.; Fernandez, J.; Szabo, G.; Albillos, A.; Louvet, A.; Jalan, R.; Moreau, R.; Moreno, C. Sepsis in alcohol-related liver disease. *J. Hepatol.* **2017**, *67*, 1031–1050. [[CrossRef](#)]
27. Yamanaka, T.; Yamane, K.; Furukawa, T.; Matsumoto-Mashimo, C.; Sugimori, C.; Nambu, T.; Obata, N.; Walker, C.B.; Leung, K.P.; Fukushima, H. Comparison of the virulence of exopolysaccharide-producing *Prevotella intermedia* to exopolysaccharide non-producing periodontopathic organisms. *BMC Infect. Dis.* **2011**, *11*, 228. [[CrossRef](#)]

28. Naruishi, K.; Omori, K.; Maeda, H.; Sonoi, N.; Funakoshi, K.; Hirai, K.; Ishii, M.; Kubo, K.; Kobayashi, H.; Tomiyama, T.; et al. Immune responses to *Porphyromonas gingivalis* infection suppress systemic inflammatory response in experimental murine model. *J. Biol. Regul. Homeost. Agents* **2011**, *25*, 195–202.
29. Mookerjee, R.P.; Stadlbauer, V.; Lidder, S.; Wright, G.A.; Hodges, S.J.; Davies, N.A.; Jalan, R. Neutrophil dysfunction in alcoholic hepatitis superimposed on cirrhosis is reversible and predicts the outcome. *Hepatology* **2007**, *46*, 831–840. [[CrossRef](#)]
30. Wieser, V.; Tymoszek, P.; Adolph, T.E.; Grander, C.; Grabherr, F.; Enrich, B.; Pfister, A.; Lichtmanegger, L.; Gerner, R.; Drach, M.; et al. Lipocalin 2 drives neutrophilic inflammation in alcoholic liver disease. *J. Hepatol.* **2016**, *64*, 872–880. [[CrossRef](#)]
31. Tarantino, G.; Scalera, A.; Finelli, C. Liver-spleen axis: Intersection between immunity, infections and metabolism. *World J. Gastroenterol.* **2013**, *19*, 3534–3542. [[CrossRef](#)]
32. Krenkel, O.; Puengel, T.; Govaere, O.; Abdallah, A.T.; Mossanen, J.C.; Kohlhepp, M.; Liepelt, A.; Lefebvre, E.; Luedde, T.; Hellerbrand, C.; et al. Therapeutic inhibition of inflammatory monocyte recruitment reduces steatohepatitis and liver fibrosis. *Hepatology* **2018**, *67*, 1270–1283. [[CrossRef](#)]
33. Roohani, S.; Tacke, F. Liver Injury and the Macrophage Issue: Molecular and Mechanistic Facts and Their Clinical Relevance. *Int. J. Mol. Sci.* **2021**, *22*, 7249. [[CrossRef](#)]
34. Olefsky, J.M.; Glass, C.K. Macrophages, inflammation, and insulin resistance. *Annu. Rev. Physiol.* **2010**, *72*, 219–246. [[CrossRef](#)]
35. Burns, E.; Eliyahu, T.; Uematsu, S.; Akira, S.; Nussbaum, G. TLR2-dependent inflammatory response to *Porphyromonas gingivalis* is MyD88 independent, whereas MyD88 is required to clear infection. *J. Immunol.* **2010**, *184*, 1455–1462. [[CrossRef](#)]
36. Akira, S.; Takeda, K. Toll-like receptor signalling. *Nat. Rev. Immunol.* **2004**, *4*, 499–511. [[CrossRef](#)]
37. Lamont, R.J.; Koo, H.; Hajishengallis, G. The oral microbiota: Dynamic communities and host interactions. *Nat. Rev. Microbiol.* **2018**, *16*, 745–759. [[CrossRef](#)]
38. Jaeschke, H. Neutrophil-mediated tissue injury in alcoholic hepatitis. *Alcohol* **2002**, *27*, 23–27. [[CrossRef](#)]
39. Guardado, S.; Ojeda-Juarez, D.; Kaul, M.; Nordgren, T.M. Comprehensive review of lipocalin 2-mediated effects in lung inflammation. *Am. J. Physiol. Lung Cell. Mol. Physiol.* **2021**, *321*, L726–L733. [[CrossRef](#)]
40. Sadik, C.D.; Luster, A.D. Lipid-cytokine-chemokine cascades orchestrate leukocyte recruitment in inflammation. *J. Leukoc. Biol.* **2012**, *91*, 207–215. [[CrossRef](#)]
41. Xu, M.J.; Feng, D.; Wu, H.; Wang, H.; Chan, Y.; Kolls, J.; Borregaard, N.; Porse, B.; Berger, T.; Mak, T.W.; et al. Liver is the major source of elevated serum lipocalin-2 levels after bacterial infection or partial hepatectomy: A critical role for IL-6/STAT3. *Hepatology* **2015**, *61*, 692–702. [[CrossRef](#)]
42. Olsen, I.; Hajishengallis, G. Major neutrophil functions subverted by *Porphyromonas gingivalis*. *J. Oral Microbiol.* **2016**, *8*, 30936. [[CrossRef](#)]
43. Miralda, I.; Uriarte, S.M.; McLeish, K.R. Multiple Phenotypic Changes Define Neutrophil Priming. *Front. Cell. Infect. Microbiol.* **2017**, *7*, 217. [[CrossRef](#)]
44. Ellis, T.N.; Beaman, B.L. Interferon-gamma activation of polymorphonuclear neutrophil function. *Immunology* **2004**, *112*, 2–12. [[CrossRef](#)]
45. Panday, A.; Sahoo, M.K.; Osorio, D.; Batra, S. NADPH oxidases: An overview from structure to innate immunity-associated pathologies. *Cell. Mol. Immunol.* **2015**, *12*, 5–23. [[CrossRef](#)]
46. Borregaard, N. Neutrophils, from marrow to microbes. *Immunity* **2010**, *33*, 657–670. [[CrossRef](#)]
47. Gahmberg, C.G. Leukocyte adhesion: CD11/CD18 integrins and intercellular adhesion molecules. *Curr. Opin. Cell Biol.* **1997**, *9*, 643–650. [[CrossRef](#)]
48. Vandendriessche, S.; Cambier, S.; Proost, P.; Marques, P.E. Complement Receptors and Their Role in Leukocyte Recruitment and Phagocytosis. *Front. Cell Dev. Biol.* **2021**, *9*, 624025. [[CrossRef](#)]
49. El Kebir, D.; Filep, J.G. Modulation of Neutrophil Apoptosis and the Resolution of Inflammation through beta2 Integrins. *Front. Immunol.* **2013**, *4*, 60. [[CrossRef](#)]
50. DeLeo, F.R. Modulation of phagocyte apoptosis by bacterial pathogens. *Apoptosis* **2004**, *9*, 399–413. [[CrossRef](#)]
51. Wang, Y.; Branicky, R.; Noe, A.; Hekimi, S. Superoxide dismutases: Dual roles in controlling ROS damage and regulating ROS signaling. *J. Cell Biol.* **2018**, *217*, 1915–1928. [[CrossRef](#)]
52. Pias, E.K.; Ekshyyan, O.Y.; Rhoads, C.A.; Fuseler, J.; Harrison, L.; Aw, T.Y. Differential effects of superoxide dismutase isoform expression on hydrogen peroxide-induced apoptosis in PC-12 cells. *J. Biol. Chem.* **2003**, *278*, 13294–13301. [[CrossRef](#)]
53. El Kebir, D.; Damlaj, A.; Filep, J.G. Toll-like receptor 9 signaling delays neutrophil apoptosis by increasing transcription of Mcl-1. *PLoS ONE* **2014**, *9*, e87006. [[CrossRef](#)]
54. Coxon, A.; Rieu, P.; Barkalow, F.J.; Askari, S.; Sharpe, A.H.; von Andrian, U.H.; Arnaout, M.A.; Mayadas, T.N. A novel role for the beta 2 integrin CD11b/CD18 in neutrophil apoptosis: A homeostatic mechanism in inflammation. *Immunity* **1996**, *5*, 653–666. [[CrossRef](#)]
55. Kumar, V. The complement system, toll-like receptors and inflammasomes in host defense: Three musketeers' one target. *Int. Rev. Immunol.* **2019**, *38*, 131–156. [[CrossRef](#)]
56. Yu, S.; Wang, D.; Huang, L.; Zhang, Y.; Luo, R.; Adah, D.; Tang, Y.; Zhao, K.; Lu, B. The complement receptor C5aR2 promotes protein kinase R expression and contributes to NLRP3 inflammasome activation and HMGB1 release from macrophages. *J. Biol. Chem.* **2019**, *294*, 8384–8394. [[CrossRef](#)]

57. Wu, G.; Zhu, Q.; Zeng, J.; Gu, X.; Miao, Y.; Xu, W.; Lv, T.; Song, Y. Extracellular mitochondrial DNA promote NLRP3 inflammasome activation and induce acute lung injury through TLR9 and NF-kappaB. *J. Thorac. Dis.* **2019**, *11*, 4816–4828. [[CrossRef](#)]
58. Kourtzelis, I.; Hajishengallis, G.; Chavakis, T. Phagocytosis of Apoptotic Cells in Resolution of Inflammation. *Front. Immunol.* **2020**, *11*, 553. [[CrossRef](#)]
59. Castro, S.A.; Collighan, R.; Lambert, P.A.; Dias, I.H.; Chauhan, P.; Bland, C.E.; Milic, I.; Milward, M.R.; Cooper, P.R.; Devitt, A. *Porphyromonas gingivalis* gingipains cause defective macrophage migration towards apoptotic cells and inhibit phagocytosis of primary apoptotic neutrophils. *Cell Death Dis.* **2017**, *8*, e2644. [[CrossRef](#)]
60. Yoneda, M.; Hirofuji, T.; Anan, H.; Matsumoto, A.; Hamachi, T.; Nakayama, K.; Maeda, K. Mixed infection of *Porphyromonas gingivalis* and *Bacteroides forsythus* in a murine abscess model: Involvement of gingipains in a synergistic effect. *J. Periodontal Res.* **2001**, *36*, 237–243. [[CrossRef](#)]
61. Talukdar, S.; Oh, D.Y.; Bandyopadhyay, G.; Li, D.; Xu, J.; McNelis, J.; Lu, M.; Li, P.; Yan, Q.; Zhu, Y.; et al. Neutrophils mediate insulin resistance in mice fed a high-fat diet through secreted elastase. *Nat. Med.* **2012**, *18*, 1407–1412. [[CrossRef](#)]
62. Liangpunsakul, S.; Ross, R.A.; Crabb, D.W. Activation of carbohydrate response element-binding protein by ethanol. *J. Investig. Med.* **2013**, *61*, 270–277. [[CrossRef](#)]
63. Iizuka, K.; Takao, K.; Yabe, D. ChREBP-Mediated Regulation of Lipid Metabolism: Involvement of the Gut Microbiota, Liver, and Adipose Tissue. *Front. Endocrinol.* **2020**, *11*, 587189. [[CrossRef](#)]

Disclaimer/Publisher’s Note: The statements, opinions and data contained in all publications are solely those of the individual author(s) and contributor(s) and not of MDPI and/or the editor(s). MDPI and/or the editor(s) disclaim responsibility for any injury to people or property resulting from any ideas, methods, instructions or products referred to in the content.